pH and Urea Dependence of Amide Hydrogen−Deuterium Exchange Rates in the β-Trefoil Protein Hisactophilin†

R. Scott Houliston,‡ Chengsong Liu, Laila M. R. Singh,§ and Elizabeth M. Meiering*

Guelph-Waterloo Centre for Graduate Work in Chemistry and Biochemistry, Department of Chemistry, University of Waterloo, Waterloo, Ontario, Canada N2L 3G1

Received July 31, 2001; Revised Manuscript Received November 12, 2001

ABSTRACT: Amide hydrogen/deuterium exchange rates were measured as a function of pH and urea for 37 slowly exchanging amides in the β-trefoil protein hisactophilin. The rank order of exchange rates is generally maintained under different solution conditions, and trends in the pH and urea dependence of exchange rates are correlated with the rank order of exchange rates. The observed trends are consistent with the expected behavior for exchange of different amides via global and/or local unfolding. Analysis of the pH dependence of exchange in terms of rate constants for structural opening and closing reveals a wide range of rates in different parts of the hisactophilin structure. The slowest exchanging amides have the slowest opening and closing rates. Many of the slowest exchanging amides are located in trefoil 2, but there are also some slow exchanging amides in trefoils 1 and 3. Slow exchangers tend to be near the interface between the β-barrel and the β-hairpin triplet portions of this single-domain structure. The pattern of exchange behaviour in hisactophilin is similar to that observed previously in interleukin-1β, indicating that exchange properties may be conserved among β-trefoil proteins. Comparisons of opening and closing rates in hisactophilin with rates obtained for other proteins reveal clear trends for opening rates; however, trends in closing rates are less apparent, perhaps due to inaccuracies in the values used for intrinsic exchange rates in the data fitting. On the basis of the pH and urea dependence of exchange rates and optical measurements of stability and folding, EX2 is the main exchange mechanism in hisactophilin, but there is also evidence for varying levels of EX1 exchange at low and high pH and high urea concentrations. Equilibrium intermediates in which subglobal portions of structure are cooperatively disrupted are not apparent from analysis of the urea dependence of exchange rates. There is, however, a strong correlation between the Gibbs free energy of opening and the denaturant dependence of opening for all amides, which suggests exchange from a continuum of states with different levels of structure. Intermediates are not very prominent either in equilibrium exchange experiments or in quenched-flow kinetic studies; hence, hisactophilin may not form partially folded states as readily as IL-1β and other β-trefoil proteins.

Hisactophilin is a histidine-rich actin binding protein from the slime mold *Dictyostelium discoideum* (*1*, *2*). The structure of hisactophilin (*3*) (Figure 1) is representative of the β-trefoil fold (*4*), which consists of three sequential trefoil units, each containing four β-strands. The β-strands form a β-hairpin triplet, which packs against one end of a six-stranded, antiparallel β-barrel (*4*). This interesting all-β structure is adopted by various protein superfamilies with unrelated functions, including cytokines, such as interleukin-1β (IL-1β)[1] and fibroblast growth factors; ricin B-like; agglutinin; Kunitz protease inhibitors; and the actin binding protein hisactophilin (*4*−*6*). We have undertaken in-depth studies of the folding and dynamics of hisactophilin to gain insights into the molecular determinants of the β-trefoil fold and the principles of folding of all-β proteins (*7*, *8*).

Measurement of the rates of hydrogen−deuterium (H/D) exchange of backbone amide protons in proteins is a powerful tool for investigating protein folding, stability, and dynamics at atomic resolution (reviewed in refs *9*−*12*). The exchange of amide protons with solvent deuterons can be described using the general two-step model of Linderstrom-Lang (*13*) refined by Hvidt and Nielsen (*14*):

$$\text{closed}^{H} \underset{k_{cl}}{\overset{k_{op}}{\rightleftharpoons}} \text{open}^{H} \xrightarrow[D_2O]{k_{int}} \text{exchanged} \qquad (1)$$

in which closed^{H} represents the closed, protonated state of the protein, open^{H} represents the open, i.e., exchange competent, protonated state of the protein, exchanged represents the deuterated protein, k_{op} is the rate constant for opening, k_{cl} is the rate constant for closing, and k_{int} is the intrinsic rate constant for amide H/D exchange in the open

† This work was supported by a grant from the Natural Sciences and Engineering Research Council of Canada.

* To whom correspondence should be addressed. E-mail: meiering@uwaterloo.ca. Fax: (519) 746-0435. Phone: (519) 885-1211.

‡ Present address: Department of Chemistry and Biochemistry, University of Guelph, Guelph, Ontario, Canada.

§ Present address: Department of Biochemistry, Simon Fraser University, Burnaby, British Columbia, Canada.

[1] Abbreviations: NMR, nuclear magnetic resonance; DSC, differential scanning calorimetry; NH, amide proton; HSQC, heteronuclear single-quantum correlation; ACBP, acyl-coenzyme A binding protein; OMTKY3, turkey ovomucoid third domain; IL-1β, interleukin-1β; BEM, binomial extrapolation method; LEM, linear extrapolation method.

10.1021/bi0115838 CCC: $22.00
Published on Web 01/04/2002

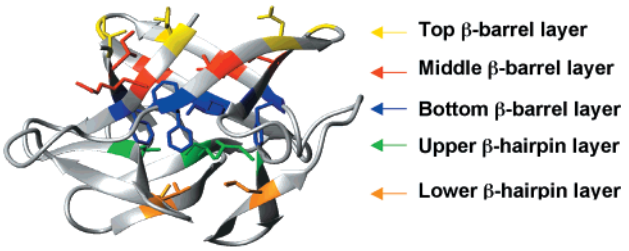

FIGURE 1: Ribbon diagram of the structure of hisactophilin. The β-trefoil structure consists of 12 β-strands, which can be grouped into three trefoil units each containing four sequential β-strands. Each trefoil contributes two strands to a six-stranded β-barrel (shown at the top of the structure) and two strands to the triangular β-hairpin triplet (shown at the bottom of the structure) that caps one end of the β-barrel. Residues participating in the three layers of the β-barrel or in the two β-hairpin layers are colored, and their side chains are shown as stick representations. Residues in the top layer (G2, N38, G41, H78, G81, and I117) of the β-barrel are colored yellow; those in the middle layer (R4, V36, V43, L76, V83, and G115) are red, and those in the bottom layer (F6, F34, L45, F74, I85, and F113) are blue. The three residues forming the upper β-hairpin layer (L14, L53, and I93) are colored green, and those forming the lower β-hairpin layer (V21, L63, and S102) are orange. The 18 residues comprising the middle and bottom β-barrel layers and the upper and lower β-hairpin layers are structurally conserved as medium or large hydrophobic residues in different β-trefoil proteins (*4*). The amides that exchange by global unfolding and correspond to the slow exchange core (A44, L45, K46, S54, Y62, F74, I85, K86, I93, S94, F113, and E114; see Tables 2 and 3) are located near the interface between the β-barrel and β-hairpin portions of the structure. With the exception of Y62, these amides are all in the bottom β-barrel layer, in the upper β-hairpin layer, or directly adjacent in primary sequence to residues in these layers. The figure was produced using the program MOLMOL (*65*) and the NMR structure of hisactophilin (PDB entry 1hcd).

state. Under conditions favoring the native state (i.e., $k_{cl} \gg k_{op}$), the observed rate constant for the overall process, k_{obs}, is given by

$$k_{obs} = \frac{k_{op}k_{int}}{k_{cl} + k_{int}} \tag{2}$$

There are two kinetic limits for the exchange process. At the EX1 limit, $k_{cl} \ll k_{int}$ so that k_{obs} depends on only k_{op}:

$$k_{obs} = k_{op} \tag{3}$$

At the EX2 limit, $k_{cl} \gg k_{int}$ so that k_{obs} is proportional to k_{int} and the equilibrium constant for opening, K_{op}:

$$k_{obs} = \frac{k_{op}}{k_{cl}}k_{int} = K_{op}k_{int} \tag{4}$$

k_{int} is pH-dependent, so measurements of k_{obs} as a function of pH can be used to determine k_{op} and k_{cl} (*15*−*19*). This is a powerful method for quantitative analysis of the dynamics of individual amide groups located throughout a protein structure. Values of k_{cl} can also be compared with values of k_{int} to determine the exchange mechanism of individual amides.

The structure and stability of exchange competent states in proteins can be investigated further by "native state exchange experiments" in which the urea dependence of exchange rates is measured under EX2 conditions (for reviews, see refs *12* and *20*). The apparent Gibbs free energy of opening, ΔG_{ex}, is determined by assuming that k_{int} is the same in the open state as in model peptides (*21*) and using the relation

$$\Delta G_{ex} = -RT \ln K_{op} = -RT \ln(k_{obs}/k_{int}) \tag{5}$$

where R is the gas constant and T is the absolute temperature. Measurements of k_{obs} as a function of denaturant concentration are analyzed using a two-process model in which exchange occurs through either (1) global unfolding, which is characterized by K_{op}^{glob} and depends on denaturant concentration according to m^{glob}, or (2) local unfolding, which is characterized by K_{op}^{loc} and is independent of denaturant concentration. Incorporation of these two types of openings into eq 5 gives

$$\Delta G_{ex} = -RT \ln(K_{op}^{loc} + K_{op}^{glob} e^{m^{glob}[U]/RT}) \tag{6}$$

where [U] is the concentration of a denaturant, such as urea or guanidinium hydrochloride. K_{op}^{glob} and m^{glob} may correspond to subglobal openings rather than global unfolding.

In this paper, we report extensive amide exchange measurements for 37 slowly exchanging amides in hisactophilin as a function of pH and urea concentration. The data are analyzed in terms of opening and closing rate constants and equilibria, providing a detailed characterization of structural fluctuations in hisactophilin.

EXPERIMENTAL PROCEDURES

Urea Denaturation Curves and Kinetics. Deuterated urea was obtained from Sigma/Aldrich or was prepared by repeated lyophilization of protonated urea after dissolution and incubation in D_2O. The extent of deuteration was confirmed as >99% by NMR. Recombinant hisactophilin and buffers were prepared as described previously (*8*) with the following modifications. For equilibrium denaturation curves, lyophilized protein was dissolved in 500 mM potassium phosphate or sodium glycinate buffer containing 10 mM DTT and 10 mM EDTA in D_2O (99.9% purity, Cambridge Isotope Laboratories), and then diluted 10-fold using D_2O and 10 M deuterated urea (final protein concentration of ~0.2−0.3 mg/mL). Denaturation curve data were fit as described previously (*8*) to a two-state transition between the native and denatured state using the binomial extrapolation method (BEM) according to the equation

$$Y = \frac{Y_N - [Y_N - (Y_U + S_U[\text{urea}])]e^{-(\Delta G_u^o + m_1[\text{urea}] - m_2[\text{urea}]^2)/RT}}{1 + e^{-(\Delta G_u^o + m_1[\text{urea}] - m_2[\text{urea}]^2)/RT}} \tag{7}$$

where Y is the observed fluorescence, Y_N is the fluorescence of the native state, Y_U is the fluorescence of the unfolded state in the absence of urea, S_U is the denaturant dependence of the fluorescence of the unfolded state, ΔG_u^o is the Gibbs free energy of unfolding in the absence of denaturant, m_1 and m_2 are constants describing the denaturant dependence of the Gibbs free energy of unfolding, R is the gas constant, and T is the absolute temperature. m_2 was fixed at 0.072 on the basis of the combined analysis of urea and thermal denaturation data (*8*).

For kinetic experiments, concentrated protein solutions were prepared as described above, and kinetics were initiated

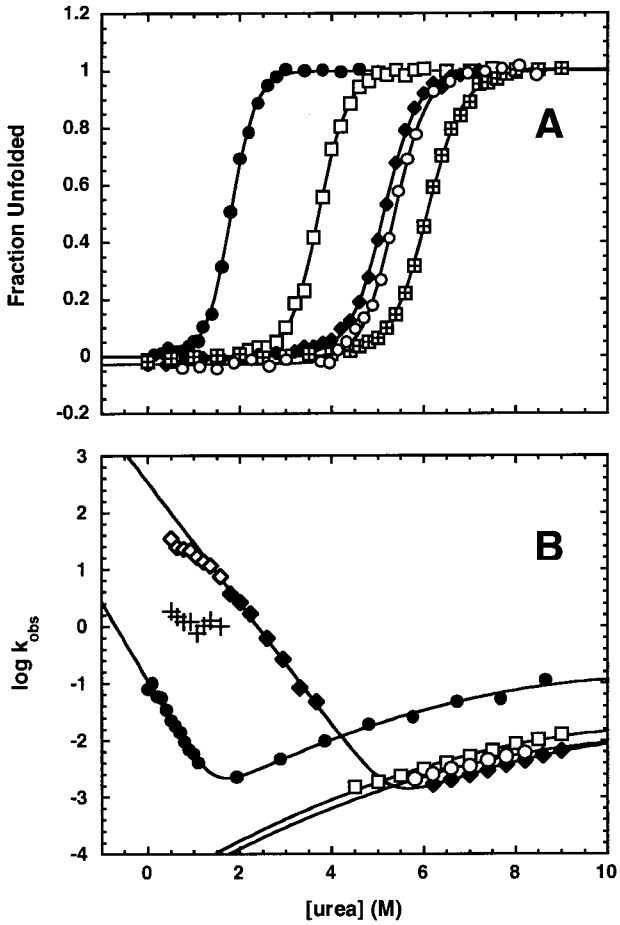

FIGURE 2: Fluorescence-monitored stability and kinetics of hisactophilin in D_2O as a function of pH. (A) Equilibrium urea denaturation curves. (B) Kinetics of unfolding and refolding. Data are for pH 5.9 (●), 6.8 (□), 7.8 (◆, ◇, and +), 8.7 (⊞), and 9.7 (○). Solid lines in panel A represent fits of the data to a two-state transition between the native and unfolded states (eq 7). Solid lines in panel B represent fits of the data to a two-state transition between the native and unfolded states considering only unfolding data (eq 8) for pH 6.8 and 9.7, and unfolding and refolding data (eq 9) for pH 5.9 and 7.8. Data below 2.0 M urea at pH 7.8 were excluded from the two-state fit due to the occurrence of double-exponential refolding kinetics in these experiments (◇ and + represent rates for the fast and slow phase, respectively) and in quenched-flow experiments, which provide evidence for formation of a folding intermediate (*22*). The fast phase accounts for ~80−90% of the total fluorescence change. Amplitudes for kinetic data correspond to values expected on the basis of equilibrium experiments. This further validates analysis of the kinetic data using the two-state model. Values obtained from the fits are summarized in Table 1.

by dilution (usually 10-fold) of the protein solution. For rates slower than ~0.01 s^{-1}, reactions were initiated by manual mixing, while faster rates were measured by stopped-flow, using an SFM4/Q instrument (Molecular Kinetics, Pullman, WA) interfaced to the Fluorolog-22/Neslab waterbath system. Raw kinetic data were fit using Biokine 2.10 software (Molecular Kinetics). Kinetic data are generally single-exponential and consistent with a two-state transition between the native and denatured states, except at low denaturant concentrations at pH 7.8, where double-exponential kinetics are observed in fluorescence and quenched-flow NMR experiments and there is evidence for formation of a kinetic folding intermediate (Figure 2B; *22*). In this paper, we are concerned with the two-state transition; non-two-state behavior is described in detail elsewhere (*22*). The natural logarithm of the unfolding rate for hisactophilin has a nonlinear denaturant dependence in D_2O (Figure 2B) and in H_2O (*22*). Similar behavior has been observed for other proteins, for which two-state unfolding has been fit using a second-order polynomial (*23*−*25*). Hisactophilin unfolding rates were therefore fit using

$$\log k_{unf}([\text{urea}]) = \log k^{o}_{unf} + [m_{unf,1}/(2.303RT)][\text{urea}] - [m_{unf,2}/(2.303RT)][\text{urea}]^2 \quad (8)$$

and complete kinetic data were fit using

$$\log k_{obs}([\text{urea}]) = \log\{k^{o}_{unf} \times 10^{[m_{unf,1}/(2.303RT)][\text{urea}]-[m_{unf,2}/(2.303RT)][\text{urea}]^2} + k^{o}_{ref} \times 10^{-[m_{ref}/(2.303RT)][\text{urea}]}\} \quad (9)$$

where k^{o}_{unf} and k^{o}_{ref} are the unfolding and refolding rate constants in the absence of denaturant, respectively, m_{ref} describes the linear denaturant dependence of the natural logarithm of the refolding rate, and $m_{unf,1}$ and $m_{unf,2}$ describe a quadratic denaturant dependence for the natural logarithm of the unfolding rate. $m_{unf,2}$ was fixed at 0.0473, which is the average value from fitting data for many different unfolding experiments (*22*). ΔG^{o}_{u} was then calculated from kinetic data using

$$\Delta G^{o}_{u} = -RT \ln \frac{k^{o}_{unf}}{k^{o}_{ref}} \quad (10)$$

Note that there is good agreement between fitted values obtained from equilibrium data and from kinetic data using the equations for a two-state transition with nonlinear denaturant dependence (Table 1). This and the results of the amide exchange experiments (see the Results) further support analysis of equilibrium data for hisactophilin using BEM (*8*).

Amide Exchange Rate Measurements. Uniformly ^{15}N-enriched hisactophilin for NMR samples was prepared as described previously (*7*). For measurement of the pH dependence of amide exchange rates, purified protein was exchanged into 50 mM potassium phosphate buffer at pH 5.9, 6.8, and 7.8 or 50 mM glycine buffer at pH 8.7 and 9.7 and then lyophilized. Amide hydrogen−deuterium exchange was initiated by redissolving the sample in D_2O to the same volume that existed prior to lyophilization. For exchange measurements in urea, an appropriate volume of a stock solution of deuterated urea in D_2O was added upon redissolving the sample in D_2O. The protein concentration for the NMR experiments (~13 mg/mL) is significantly higher than that for fluorescence-monitored experiments (~0.3 mg/mL); however, hisactophilin stability does not change with protein concentration over this range (*8*; C. Liu and E. M. Meiering, unpublished data).

Amide exchange rates were determined from the rate of decay of NH cross-peak intensity in successive $^{1}H-^{15}N$ HSQC spectra, which were acquired on a Bruker AMX500 spectrometer using gradients for artifact and water suppression (*26*). Each spectrum took 12.5 min to acquire. After the protein had been redissolved, samples were thermally equilibrated in the magnet. Acquisition of the first spectrum was initiated approximately 15 min after the protein had been

Table 1: Summary of Equilibrium and Kinetic Parameters for Hisactophilin in D_2O[a]

pH[b]	method		ΔG_u^o (kcal/mol)	m_1 (kcal mol^{-1} M^{-1})	C_{mid} (M)	log k_{ref}^o (s^{-1})	m_{ref} (kcal mol^{-1} M^{-1})	log k_{unf}^o (s^{-1})	$m_{unf,1}$ (kcal mol^{-1} M^{-1})
5.9	equilibrium	BEM	4.04 ± 0.23	2.37 ± 0.12	1.80 ± 0.02	–	–	–	–
		LEM	3.93 ± 0.26	2.17 ± 0.13	1.81 ± 0.02				
	kinetic	–	3.44 ± 0.14	2.46 ± 0.01	1.42 ± 0.12	−0.96 (0.04)	1.84 ± 0.09	3.51 (0.07)	0.62 ± 0.01
6.8	equilibrium	BEM	8.18 ± 0.29	2.46 ± 0.08	3.73 ± 0.01				
		LEM	7.13 ± 0.29	1.91 ± 0.07	3.73 ± 0.02				
	kinetic	–	–	–	–	*1.34 (0.26)*	*1.77 ± 0.09*	−4.67 (0.06)	0.65 ± 0.01
7.8	equilibrium	BEM	10.84 ± 0.29	2.47 ± 0.06	5.17 ± 0.02	–	–	–	–
		LEM	9.04 ± 0.27	1.75 ± 0.05	5.16 ± 0.02				
	kinetic	–	10.51 ± 0.28	2.14 ± 0.06	5.27 ± 0.33	2.53 (0.07)	1.43 ± 0.04	−5.30 (0.15)	0.71 ± 0.02
8.7	equilibrium	BEM	12.14 ± 0.28	2.44 ± 0.05	6.07 ± 0.02	–	–	–	–
		LEM	9.61 ± 0.08	1.59 ± 0.05	6.06 ± 0.01				
9.7	equilibrium	BEM	11.27 ± 0.57	2.48 ± 0.11	5.39 ± 0.03	–	–	–	–
		LEM	9.27 ± 0.56	1.72 ± 0.10	5.38 ± 0.03				
	kinetic	–	–	–	–	*3.36 (0.24)*	*1.82 ± 0.13*	−5.04 (0.12)	0.66 ± 0.02

[a] Equilibrium values were obtained from fitting urea denaturation curve data in Figure 2A to eq 7 with an m_2 of 0.072 for the binomial extrapolation method (BEM) and an m_2 of 0 for the linear extrapolation method (LEM). Previous studies have demonstrated significant nonlinear urea dependence of ΔG_u for hisactophilin, which can be fit using BEM (*8*). Values of ΔG_u^o from BEM analysis of equilibrium denaturation agree with values obtained from kinetics (see above), and are the same or slightly smaller than values of ΔG_{ex} obtained from amide exchange data (Table 2 and Supporting Information). In contrast, LEM analysis of urea denaturation curves gives considerably lower values for ΔG_u^o than other methods (ref *8* and above). The discrepancy between values obtained by the LEM and BEM increases systematically as protein stability increases and longer extrapolations are required to obtain ΔG_u^o. Thus, the data presented here provide further support for analysis of the urea dependence of ΔG_u by BEM rather than LEM. C_{mid} corresponds to a ΔG_u of 0. Kinetic fitted values were obtained by fitting unfolding and refolding rates in Figure 2B to eq 9 (pH 5.9 and 7.8) or fitting unfolding rates to eq 8 (pH 6.8 and 9.7), with an $m_{unf,2}$ of 0.0473, and then calculating refolding parameters (given in italics) by combining eqs 7 and 8. Error estimates for all fitted values are from the fitting program. For the log k_{unf}^o and log k_{ref}^o values, numbers in parentheses represent the error estimates corresponding to the maximum estimated rate constants. [b] pH values in all tables and figures correspond to the pH reading of the D_2O solutions, uncorrected for the isotope effect.

dissolved in D_2O. Spectra were recorded continuously for several hours and then at increasing time intervals for up to 110 days after initiation of exchange. NMR data were processed using Felix97 software (MSI) on an Indigo II workstation (Silicon Graphics, Inc.).

Values of k_{obs} were obtained by integrating cross-peak volumes using Felix97 and fitting the data to a single-exponential decay. Values of k_{int} were calculated on the basis of measurements of exchange rates in model peptides (*21*) using the program HX-predict (*27*). Values of k_{op} and k_{cl} for each amide were determined by fitting k_{obs} versus pH to eq 2 as described previously (*18*). For exchange experiments as a function of urea concentration, ΔG_{ex} values were calculated from k_{obs} and k_{int} using eq 5, and then K_{op}^{glob}, K_{op}^{loc}, and m^{glob} values were determined by fitting ΔG_{ex} versus urea concentration to eq 6.

Except when otherwise noted, fitting of data to the various equations was performed using nonlinear least-squares regression by the program Kaleidagraph (Synergy Software). Reported pH values for experiments are for pH_{read}, which is uncorrected for the isotope effect.

RESULTS

Urea Denaturation Curves. The thermodynamic stability of hisactophilin was measured using fluorescence-monitored urea denaturation curves in D_2O (Figure 2A) at the same pH values used for exchange experiments (see below). The denaturation curves are well fit by a two-state transition between the native and denatured states (Table 1). The denaturation data indicate that hisactophilin stability increases markedly from pH 5.9 to 7.8, and is roughly constant from pH 7.8 to 9.7. These results are very similar to the pH dependence of hisactophilin stability measured in H_2O (*8*); however, stability is slightly higher (~1−2 kcal/mol) in D_2O than in H_2O, as has been observed for other proteins (*28*−*31*).

Rates of fluorescence-monitored global unfolding and refolding of hisactophilin were also measured in D_2O at various pHs (Figure 2B). The kinetic data are also consistent with a two-state transition (see Experimental Procedures), except at low denaturant concentrations at pH 7.8, where there is evidence for formation of a folding intermediate (Figure 2B and Table 1; *22*). The refolding rate is very strongly dependent upon pH; it increases markedly from pH 5.9 to 7.8, and then remains roughly constant from pH 7.8 to 9.7. The unfolding rate is also pH-dependent, but less so than the refolding rate. The rate of unfolding is very slow, and essentially constant at pH ≥6.8, and increases markedly below pH 6.8. As for the equilibrium data, the kinetic data parallel results for experiments conducted in H_2O (*22*).

pH Dependence of Exchange. Chemical shift assignments for backbone amide groups in hisactophilin as a function of pH have been reported previously (*7*). Using these assignments, amide exchange rates were determined at pH 5.9, 6.8, 7.8, 8.7, and 9.7. Representative exchange data are shown in Figure 3, and exchange rates are given in Table 2. Amide exchange rates in hisactophilin are strongly dependent upon pH (Figure 4). Generally, the rank order of exchange rates is maintained at the different pHs; i.e., the same residues tend to exchange most slowly at all pHs. The pH dependence of the exchange rate for a given amide is correlated with its absolute exchange rate; for the slowest exchanging amides, rates decrease markedly from pH 5.9 to 7.8 and then increase slightly up to pH 9.7 (Figure 4A), while for the most rapidly exchanging amides, the rates decrease slightly from pH 5.9 to 7.8 and then increase markedly up to pH 9.7 (Figure 4B). Exchange rates are plotted versus primary sequence and secondary structure in Figure 5. Many of the slowest

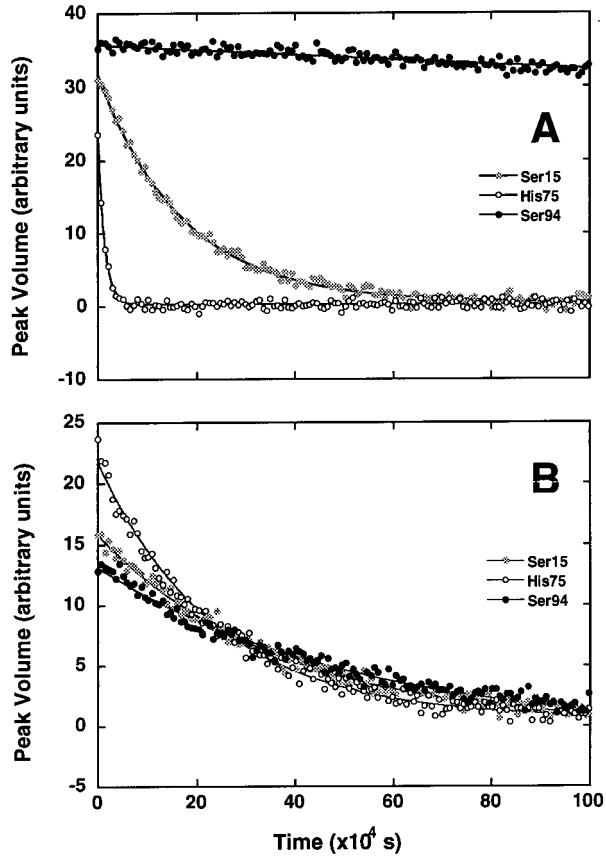

FIGURE 3: Representative decays in $^1H-^{15}N$ HSQC amide cross-peak volume with time after dissolution of fully protonated hisactophilin in D_2O at (A) pH 8.7 and (B) 5.9. Lines represent the fit of the data to a single-exponential decay using nonlinear least-squares regression.

exchanging amides are located in trefoil 2; however, there are also some slow exchangers in trefoils 1 and 3. In general, slow exchangers tend to be near the interface between the β-barrel and β-hairpin triplet portions of the structure (Figure 1).

It is generally accepted that the most slowly exchanging amides in proteins tend to exchange via global unfolding of the protein (*9*−*12*). For such amides, under EX2 conditions, ΔG_{ex} should equal ΔG_u^o measured using urea denaturation curves. ΔG_{ex} was calculated for the slowest exchanging amides in hisactophilin using eq 5 (Table 2 and Supporting Information). There is good agreement between the average ΔG_{ex} value for the slowest amides and ΔG_u^o (Table 1) at pH 6.8, 7.8, and 8.7, but at pH 5.9 and 9.7, ΔG_{ex} is larger than ΔG_u^o. These results are consistent with a predominantly EX2 exchange mechanism from pH 6.8 to 7.8, and significant occurrence of EX1 exchange at both higher and lower pH (vide infra and Discussion).

Analysis of the pH dependence of k_{obs} in terms of k_{op} and k_{cl} requires that k_{op} and k_{cl} remain constant with changing pH (*15*−*17*). The stability and global unfolding and refolding rates of hisactophilin are roughly constant from pH 7.8 to 9.7, but change considerably at lower pH (Table 1) and higher pH (C. Liu, T. Walma, and E. M. Meiering, unpublished data). Consequently, k_{obs} values from pH 7.8 to 9.7 were fit to eq 2 to determine k_{op} and k_{cl}. Note that there is very little change in the $^1H-^{15}N$ HSQC spectrum of hisactophilin from pH 7.8 to 9.7, indicating that the structure of native hisactophilin is also constant over this pH range (*7*). Fitted values of k_{op} and k_{cl} are given in Table 2.

The slowest exchanging amides in hisactophilin clearly have the smallest values for k_{op} and also tend to have the smallest values for k_{cl} (Table 2 and Figure 6A). Values of k_{cl} can be compared with values of k_{int} to elucidate the exchange mechanism for individual amides (Figure 6B). Note that the ratio of k_{cl} to k_{int} is independent of the absolute value used for k_{int} in the fitting (*17*, *32*), and so the exchange mechanism can be analyzed even when there are inaccuracies in k_{int} (vide infra). At pH 7.8, $k_{cl} > k_{int}$ for most amides, indicating that EX2 is the dominant exchange mechanism. For the fast exchangers, k_{cl} is ~2 orders of magnitude larger than k_{int}, while for the slow exchangers, k_{cl} is generally only slightly larger than k_{int}. Thus, EX1 may occur to some extent for the slowest exchangers at this pH. Since k_{int} increases 10-fold for every unit increase in pH, by pH 9.7, $k_{cl} < k_{int}$ for most amides; hence, exchange occurs predominantly via EX1.

The values of k_{op} and k_{cl} for the slowest exchanging amides are consistent with fluorescence measurements of global stability and unfolding and folding kinetics. Values of ΔG_{fit} calculated from k_{op} and k_{cl} for the slowest amides (Table 2) are very similar to the ΔG_u^o measured by fluorescence-monitored equilibrium denaturation curves (Table 1). Also, average values of k_{op} and k_{cl} for the slowest amides [log values of −6.12 (0.40) and 1.78 (0.44), respectively (Table 2)] are in reasonable agreement with the rates of global unfolding and refolding measured by fluorescence at pH 7.8 [log values of −5.30 (0.15) and 2.53 (0.07), respectively (Table 1)], considering the following experimental aspects of the determination these values. First, the global unfolding and refolding rates measured by fluorescence should be slightly faster than rates obtained by amide exchange because the former rates were measured at 20.0 °C while the latter were measured at 17.4 °C. Second, determination of global refolding and particularly unfolding rates in the absence of denaturant may have significant extrapolation errors (Figure 2B). Third, values of k_{cl} are directly dependent on values used for k_{int} in the fitting (*17*, *32*); i.e., a 10-fold increase in k_{int} causes a 10-fold increase in k_{cl}, and thus any inaccuracy in k_{int} will be reflected in k_{cl}. [Note, however, that values of k_{op} depend very little on k_{int} (*17*, *32*).] Experimental measurements of k_{int} have generally been found to agree within ~3-fold with predicted values of k_{int} for denatured proteins (*33*−*37*). Also, good agreement has been reported between rate constants for global folding and unfolding determined by amide exchange, optical methods, and saturation transfer NMR experiments for other proteins (*19* and references therein). Thus, measurement of the pH dependence of amide exchange rates appears to be a robust method for investigating rate constants for structural fluctuations in proteins (*19*).

Urea Dependence of Exchange Rates. Analysis of the denaturant dependence of amide exchange rates in terms of structural opening equilibria requires EX2 exchange conditions. For hisactophilin, exchange is most likely to occur by EX2 at pH 7.8, i.e., the lowest pH where the protein has high thermodynamic stability and fast folding rates (Table 1). Consequently, the urea dependence of exchange was measured at pH 7.8 from 0 to 3.0 M urea (Table 3). The midpoint of the urea denaturation curve at pH 7.8 is 5.2 M

Table 2: k_{obs}, k_{op}, and k_{cl} Values for Backbone Amide Protons in Hisactophilin[a]

residue[b]	structure element[c]	log k_{obs}[d] (s^{-1})					ΔG_{ex}[e] (kcal/mol)		log k_{op}[f] (s^{-1})	log k_{cl}[f] (s^{-1})	ΔG_{fit}[g] (kcal/mol)
		pH 5.9	pH 6.8	pH 7.8	pH 8.7	pH 9.7	pH 7.8	pH 9.7			
A5	β1	−4.55	−5.52	−6.03	−5.63	−5.46	9.91	11.8	−5.46 (0.04)	2.01 (0.16)	9.92
F6	β1	−4.62	−5.59	−6.10	−5.85	−5.69	9.39	11.5	−5.71 (0.06)	1.23 (0.23)	9.23
K7	β1	−4.58	−5.44	−6.02	−5.82	−5.83	9.64	12.0	−5.81 (0.02)	1.00 (0.10)	9.06
S8	T1/2	−4.54	−5.34	−5.98	−5.62	−5.41	10.2	12.1	−5.40 (0.06)	2.38 (0.21)	10.4
L14	β2	−4.66	−5.81	−6.27	−5.62	−5.28	9.25	10.6	−5.22 (0.02)	1.85 (0.06)	9.40
S15	β2	−4.50	−5.26	−5.47	−4.74	−4.24	9.09	10.1	−4.12 (0.02)	2.86 (0.05)	9.28
A16	β2	−4.15	−4.29	−4.28	−3.28	−2.82	7.69	8.41	−2.72 (0.01)	2.93 (0.03)	7.51
F34	β3	−4.54	−5.38	−5.85	−5.24	−4.92	9.25	10.7	−4.87 (0.02)	2.22 (0.07)	9.42
H35	β3	−4.55	−5.39	−5.46	−4.99	−4.58	8.81	10.3	−4.50 (0.05)	2.45 (0.14)	9.25
E37	β3	−4.45	−4.69	−4.40	−3.46	−2.94	6.59	7.31	−2.81 (0.00)	2.10 (0.01)	6.52
V43	β5	−4.44	−5.94	−6.25	−5.48	−4.93	9.14	10.0	−4.79 (0.01)	2.22 (0.04)	9.31
A44	**β5**	**−4.71**	**−6.23**	**−7.31**	**−5.98**	**−5.69**	**11.1**	**11.6**	**−5.64 (0.03)**	**2.18 (0.11)**	**10.4**
L45	**β5**	**−4.76**	**−6.28**	**−7.37**	**−6.43**	**−6.20**	**10.6**	**11.7**	**−6.16 (0.02)**	**1.59 (0.08)**	**10.3**
K46	**β5**	**−4.60**	**−5.98**	**−7.02**	**−6.89**	**−6.53**	**10.6**	**12.6**	**−6.49 (0.12)**	**2.01 (0.34)**	**11.3**
S54	**β6**	**−4.64**	**−6.09**	**−7.08**	**−6.59**	**−6.28**	**10.5**	**12.3**	**−6.23 (0.04)**	**2.43 (0.13)**	**11.5**
Y62	**β7**	**−4.77**	**−6.31**	**−7.23**	**−6.47**	**−6.67**	**10.7**	**12.6**	**−6.55 (0.15)**	**1.03 (0.48)**	**10.1**
L73	L7/8	−4.62	−5.37	−5.49	−4.53	−3.95	8.53	9.14	−3.77 (0.02)	2.63 (0.06)	8.52
F74	**β8**	**−4.79**	**−6.40**	**−7.34**	**−7.32**	**−6.92**	**10.8**	**12.9**	**−6.88 (0.15)**	**1.85 (0.40)**	**11.6**
E77	β8	−3.71	−3.56	−3.62	fast	fast	5.46	nd[h]	nd	nd	nd
V83	β9	−4.71	−5.30	−5.29	−4.42	−3.86	7.87	8.62	−3.71 (0.00)	2.24 (0.01)	7.91
S84	β9	−4.63	−5.67	−5.97	−5.07	−4.48	9.85	10.5	−4.31 (0.00)	3.11 (0.01)	9.87
I85	**β9**	**−4.64**	**−6.03**	**−6.91**	**−6.10**	**−6.03**	**10.2**	**11.7**	**−6.00 (0.05)**	**1.37 (0.20)**	**9.80**
K86	**β9**	**−4.59**	**−6.06**	**−7.02**	**−6.14**	**−6.09**	**10.6**	**12.0**	**−6.05 (0.06)**	**1.52 (0.24)**	**10.1**
Y92	β10	−4.54	−5.83	−6.51	−5.97	−5.73	10.1	11.7	−5.70 (0.03)	1.98 (0.10)	10.2
I93	**β10**	**−4.77**	**−6.34**	**−7.28**	**−6.46**	**−6.30**	**10.4**	**11.7**	**−6.27 (0.03)**	**1.31 (0.10)**	**10.1**
S94	**β10**	**−4.59**	**−5.85**	**−6.87**	**−5.84**	**−6.02**	**10.9**	**12.5**	**−5.90 (0.15)**	**1.68 (0.50)**	**10.1**
A95	β10	−4.59	−5.48	−5.51	−4.66	−4.06	9.33	10.1	−3.89 (0.01)	3.20 (0.02)	9.42
D96	T10/11	−4.41	−4.66	−4.73	−3.88	−3.35	7.49	8.32	−3.22 (0.00)	2.46 (0.01)	7.55
H100	T10/11	−4.43	−5.76	−6.09	−5.49	−4.98	9.79	11.0	−4.86 (0.03)	2.78 (0.09)	10.2
S102	β11	−4.54	−5.30	−5.29	−4.15	−3.60	8.94	9.35	−3.45 (0.01)	3.04 (0.04)	8.63
K104	β11	−4.52	−5.08	−5.51	−4.79	−4.29	9.14	10.2	−4.17 (0.02)	2.86 (0.05)	9.35
T112	L11/12	−3.47	−3.52	−3.78	−3.16	−2.80	6.80	8.16	−2.74 (0.02)	2.54 (0.07)	7.02
F113	**β12**	**−4.76**	**−6.15**	**−7.19**	**−5.91**	**−5.71**	**11.1**	**11.8**	**−5.67 (0.05)**	**2.09 (0.16)**	**10.3**
E114	**β12**	**−4.86**	**−6.16**	**−7.15**	**−6.23**	**−5.70**	**10.5**	**11.2**	**−5.57 (0.00)**	**2.32 (0.00)**	**10.5**
I116	β12	−5.38	−6.25	−6.06	−4.66	−3.53	8.49	7.79	nd	nd	nd
I118	L12	−5.30	−4.85	−4.44	−3.49	−2.94	3.84	4.50	−2.78 (0.02)	0.097 (0.046)	3.83
"global"		**−4.7 ± 0.1**	**−6.2 ± 0.2**	**−7.2 ± 0.2**	**−6.4 ± 0.4**	**−6.2 ± 0.4**	**10.7 ± 0.3**	**12.1 ± 0.5**	**−6.12 ± 0.40**	**1.78 ± 0.44**	**10.5 ± 0.6**

[a] The following residues exchanged within the dead time of the experiment at all pH values: G2, H10, G11, H12, V21, T23, H33, H39, K42, K59, Q60, V61, S72, K82, H91, G99, V101, T103, E105, H106, D110, T111, and I117. Also, rates were too fast to measure for E77 at pH 8.7 and 9.7. [b] Residues classified as "global" exchangers (see also Figure 1) which form the slow exchange core are shown in bold type. These residues were chosen on the basis of the slowest average exchange rate, the strongest dependence of exchange on denaturant concentration, and the strongest temperature dependence for exchange rates (R. S. Houliston, L. M. R. Singh, and E. M. Meiering, unpublished data). Average exchange rates for the global exchangers and standard deviations for the averages are shown. [c] Elements of structure in the protein are numbered from the N- to C-terminus with β-strands designated by β, turns designated by T, and loops or unstructured regions designated by L. [d] Error estimates for k_{obs} obtained from the fitting program are typically ~5−10%. [e] ΔG_{ex} values were calculated using eq 5. [f] Values for k_{op} and k_{cl} were obtained by fitting k_{obs} values for pH 7.8−9.7 to eq 2. Numbers in parentheses represent the error estimates corresponding to the maximum estimated rate constants. Note that, although hisactophilin stability is somewhat higher at pH 8.7 than at pH 7.8 and 9.7, very similar values of k_{op} and k_{cl} are obtained when the pH 8.7 data are excluded, and the trends in fitted values (Figure 6) are unchanged. [g] ΔG_{fit} was calculated from $-RT \ln(k_{op}/k_{cl})$. [h] nd means not determined. Data for I116 could not be fit using eq 2.

(Table 1). Thus, on the basis of optical probes, hisactophilin is predominantly folded at the urea concentrations used for exchange rate measurements.

Representative plots of log k_{obs} versus urea concentration are shown in Figure 7. Again, the rank order of exchange rates is generally maintained for different urea concentrations, and trends in the urea dependence of exchange are correlated with the absolute exchange rate. For the most slowly exchanging amides, log k_{obs} has a strong, linear dependence on urea concentration from 0 to 2.0 M urea and a weaker urea dependence from 2.0 to 3.0 M urea (Figure 7A), while for the most rapidly exchanging amides, log k_{obs} has a much weaker, roughly linear, urea dependence over the entire range of urea concentrations (Figure 7B). The change in urea dependence of exchange with increasing urea concentration for the slow amides suggests a change in the exchange mechanism. A switch from EX2 toward EX1 has been observed for other proteins when they are destabilized by increasing denaturant concentrations (*10*, *38*, *39*). The most common method for confirming that EX2 is maintained at all denaturant concentrations is to compare k_{obs} at different pHs. This is problematic for hisactophilin because protein stability and k_{op} and k_{cl} change significantly below pH 7.8 (Table 1), while EX1 becomes significant at higher pHs (Figure 6B). An alternative approach to evaluating the mechanism is to compare experimental k_{obs} values for amides that exchange via global unfolding with expected k_{obs} values based on optically monitored measurements of global protein stability and unfolding as a function of denaturant concentration (*38*). In the EX2 limit, k_{obs} values for global amides will follow the equilibrium constant for global unfolding (eq 7), while in the EX1 limit, k_{obs} values will follow the rate of global unfolding (eq 9).

Applying this approach to hisactophilin and using the parameters in Table 1, a plot of log k_{obs} versus denaturant concentration for global amides (Figure 7A) should have an

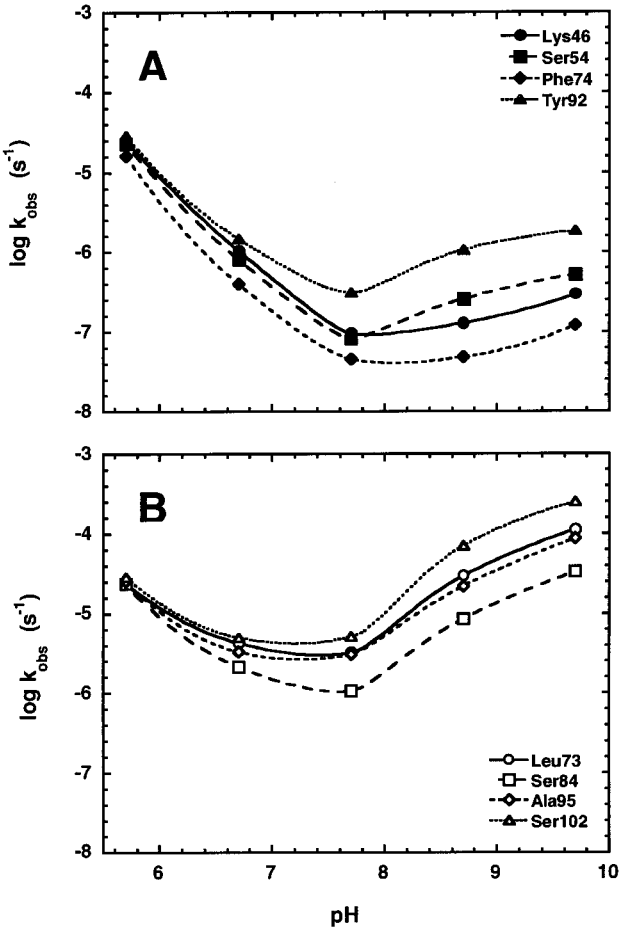

FIGURE 4: Representative pH dependence of k_{obs} for amide protons in hisactophilin. The pH profiles are very different for (A) slowly exchanging amides and (B) rapidly exchanging amides. For clarity, lines are drawn connecting data points for each residue.

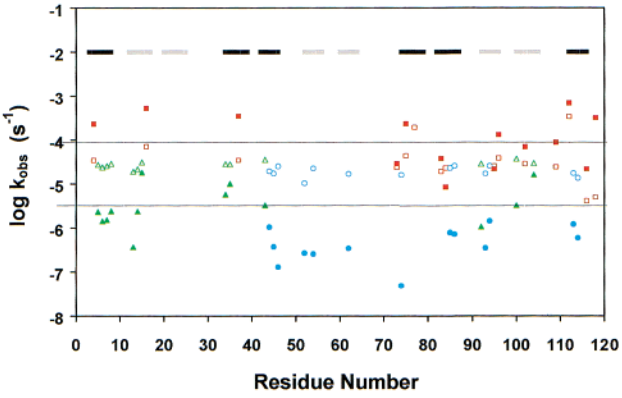

FIGURE 5: Amide exchange rates in hisactophilin at pH 5.9 (empty symbols) and pH 8.7 (filled symbols) vs residue number. Data for slow, intermediate, and fast exchanging amides are represented as blue circles, green triangles, and red squares, respectively. Black bars indicate β-barrel strands, and gray bars indicate β-hairpin strands. At pH 5.9, where hisactophilin is relatively unstable, there is a small spread in the k_{obs} values. Lines are drawn at two standard deviations above and below the mean rate at this pH. At pH 8.7, where hisactophilin is very stable, there is a much larger spread in the k_{obs} values.

average slope of ~1.6 for 0−2.0 M urea under EX2 conditions, and an average slope of ~0.40 for 2.5−3.0 M urea under EX1 conditions. For the slowest exchanging amides, the experimental slope in Figure 7A from 0 to 2.0 M urea is ~1.4, close to the predicted EX2 value, while from

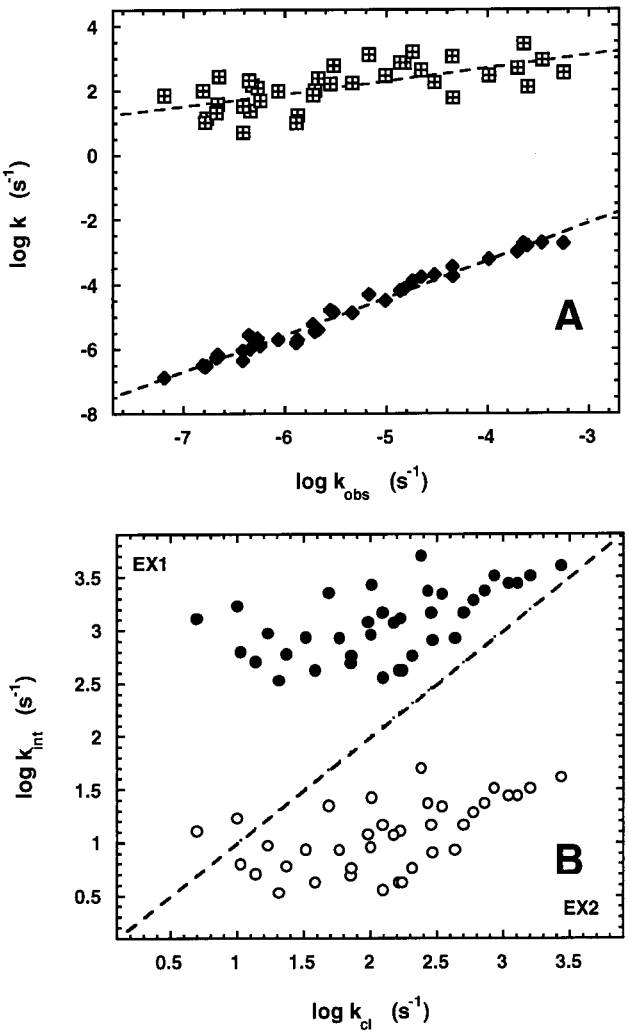

FIGURE 6: (A) Correlation of rates for structural opening (◆) and closing (⊞) with observed exchange rate for amides in hisactophilin. Log k_{obs} is the average value for the pH 7.8−9.7 data used to determine k_{op} and k_{cl}. Solid lines represent linear fits of the data by nonlinear least-squares regression. k_{op} and k_{cl} are both correlated with k_{obs} ($R = 0.99$ and 0.65, respectively). (B) Comparison of the predicted intrinsic exchange rate with the structural closing rate at pH 7.8 (○) and 9.7 (●). A line is drawn where log k_{int} = log k_{cl} to indicate where the exchange mechanism changes from primarily EX2 (points below the line) to primarily EX1 (points above the line). EX2 is the dominant mechanism of exchange at pH 7.8, while EX1 is the dominant mechanism at pH 9.7.

2.5 to 3.0 M urea, the slope is ~0.36, close to the predicted EX1 value. Also, below 2.0 M urea, ΔG_{ex} is close to ΔG_u, consistent with predominantly EX2 exchange. In 3.0 M urea, log k_{obs} is predicted to be approximately −4.00 s^{-1} for 100% EX1, and (using an average value of k_{int} for the slowest exchangers) −2.15 s^{-1} for 100% EX2, i.e., much faster for EX2. The average experimental log k_{obs} for the slowest exchangers in 3.0 M urea is approximately −4.17 s^{-1}, close to the predicted EX1 value. The slightly lower value of k_{obs} compared to k_{unf} may be due in part to a difference in the temperature used in amide exchange measurements and in kinetic unfolding measurements (17.4 and 20.0 °C, respectively) and due to extrapolation errors for k_{unf}. Thus, when both the pH and urea data are considered, the mechanism of exchange for the slowest exchanging amides in hisactophilin at pH 7.8 is predominantly EX2 at low urea concentrations and approaches the EX1 limit by 3.0 M urea. The rather

Table 3: k_{obs} vs Urea Concentration and ΔG_{op}^{loc}, ΔG_{op}^{glob}, and m^{glob} for Backbone Amide Protons in Hisactophilin

residue[a]	structure element[b]	log k_{obs}[c] (s^{-1}) 0 M urea	0.5 M urea	1.0 M urea	1.5 M urea	2.0 M urea	2.5 M urea	3.0 M urea	ΔG_{op}^{loc}[d] (kcal mol^{-1})	ΔG_{op}^{glob}[d] (kcal mol^{-1})	m^{glob}[d] (kcal mol^{-1} M^{-1})
R4	β1	−4.34	−4.26	−4.21	−4.03	−3.97	−3.88	−3.71	8.3 ± 0.8	8.3 ± 0.7	0.39 ± 0.26
A5	β1	−6.03	−5.94	−5.43	−5.07	−4.55	−4.28	−4.17	10.1 ± 0.2	10.7 ± 0.3	1.39 ± 0.19
F6	β1	−6.10	−6.01	−5.48	−5.12	−4.53	−4.27	−4.10	9.6 ± 0.2	10.3 ± 0.3	1.50 ± 0.20
K7	β1	−6.02	−5.89	−5.44	−5.02	−4.54	−4.25	−4.17	9.8 ± 0.1	10.4 ± 0.2	0.38 ± 0.13
S8	T1/2	−5.98	−5.76	−5.30	−4.94	−4.48	−4.27	−4.14	10.6 ± 0.2	10.6 ± 0.2	1.21 ± 0.09
L14	β2	−6.27	−6.15	−5.65	−5.26	−4.59	−4.32	−4.14	9.4 ± 0.1	10.3 ± 0.3	1.62 ± 0.17
S15	β2	−5.47	−5.48	−5.20	−4.88	−4.43	−4.20	−4.09	9.2 ± 0.1	10.5 ± 0.3	1.40 ± 0.17
A16	β2	−4.28	−4.28	−4.17	−3.95	−3.82	−3.73	−3.59	7.8 ± 0.2	8.8 ± 0.6	0.80 ± 0.31
F34	β3	−5.85	−5.55	−5.34	−5.02	−4.54	−4.25	−4.06	9.5 ± 0.3	9.8 ± 0.3	1.11 ± 0.18
H35	β3	−5.46	−5.45	−5.28	−5.01	−4.52	−4.26	−4.09	8.9 ± 0.1	10.9 ± 0.2	1.58 ± 0.11
E37	β3	−4.40	−4.36	−4.39	−4.20	−4.11	−4.00	−3.75	6.6 ± 0.1	8.4 ± 1.2	0.93 ± 0.59
V43	β5	−6.25	−6.19	−5.87	−5.41	−4.66	−4.32	−4.18	9.2 ± 0.1	11.0 ± 0.2	1.96 ± 0.13
A44	**β5**	**−7.31**	**−6.84**	**−5.92**	**−5.41**	**−4.63**	**−4.31**	**−4.22**	**11.8 ± 0.9**	**11.4 ± 0.3**	**1.91 ± 0.20**
L45	**β5**	**−7.37**	**−6.90**	**−5.93**	**−5.48**	**−4.65**	**−4.32**	**−4.18**	**11.4 ± 1.2**	**10.9 ± 0.3**	**1.92 ± 0.23**
K46	**β5**	**−7.02**	**−6.55**	**−5.68**	**−5.25**	**−4.55**	**−4.27**	**−4.10**	**11.7 ± 2.1**	**10.7 ± 0.3**	**1.70 ± 0.20**
S54	**β6**	**−7.08**	**−6.49**	**−5.75**	**−5.28**	**−4.58**	**−4.28**	**−4.15**	**nd**	**11.2 ± 0.2**	**1.64 ± 0.29**
Y62	**β7**	**−7.23**	**−6.66**	**−6.07**	**−5.51**	**−4.66**	**−4.32**	**−4.13**	**11.1 ± 0.5**	**11.0 ± 0.2**	**1.81 ± 0.15**
L73	L7/8	−5.49	−5.41	−5.36	−5.07	−4.58	−4.28	−4.13	8.5 ± 0.1	10.9 ± 0.3	1.73 ± 0.15
F74	**β8**	**−7.34**	**−6.89**	**−6.28**	**−5.62**	**−4.73**	**−4.36**	**−4.19**	**10.9 ± 0.2**	**11.4 ± 0.2**	**2.03 ± 0.12**
E77	β8	−3.62	−3.62	−3.51	−3.39	−3.36	−3.32	−3.20	5.8 ± 0.7	6.0 ± 1.0	0.36 ± 0.37
V83	β9	−5.29	−5.23	−5.21	−4.97	−4.54	−4.26	−4.15	7.8 ± 0.1	10.5 ± 0.3	1.75 ± 0.17
S84	β9	−5.97	−5.80	−5.47	−5.11	−4.56	−4.31	−4.17	10.0 ± 0.1	10.8 ± 0.2	1.39 ± 0.10
I85	**β9**	**−6.91**	**−6.48**	**−5.75**	**−5.27**	**−4.57**	**−4.28**	**−4.16**	**10.8 ± 0.5**	**10.5 ± 0.2**	**1.68 ± 0.13**
K86	**β9**	**−7.02**	**−6.43**	**−5.79**	**−5.31**	**−4.60**	**−4.34**	**−4.22**	**12.8 ± 8.7**	**10.6 ± 0.2**	**1.59 ± 0.10**
Y92	β10	−6.51	−6.29	−5.68	−5.26	−4.59	−4.36	−4.06	10.4 ± 0.2	10.8 ± 0.3	1.61 ± 0.16
I93	**β10**	**−7.28**	**−6.69**	**−6.03**	**−5.51**	**−4.70**	**−4.33**	**−4.15**	**11.2 ± 0.8**	**10.5 ± 0.2**	**1.76 ± 0.13**
S94	**β10**	**−6.87**	**−6.47**	**−5.69**	**−5.25**	**−4.61**	**−4.27**	**−4.17**	**11.7 ± 1.0**	**11.1 ± 0.3**	**1.61 ± 0.17**
A95	β10	−5.51	−5.52	−5.32	−4.97	−4.52	−4.25	−4.09	9.4 ± 0.1	11.1 ± 0.2	1.52 ± 0.12
D96	T10/11	−4.73	−4.72	−4.63	−4.43	−4.18	−4.06	−3.89	7.5 ± 0.1	9.1 ± 0.2	1.10 ± 0.11
H100	T10/11	−6.09	−6.02	−5.72	−5.32	−4.61	−4.30	−4.10	9.9 ± 0.1	11.6 ± 0.3	1.84 ± 0.15
S102	β11	−5.29	−5.21	−5.09	−4.79	−4.42	−4.23	−4.12	9.0 ± 0.0	10.4 ± 0.1	1.27 ± 0.06
K104	β11	−5.51	−5.31	−5.08	−4.83	−4.42	−4.20	−4.10	9.4 ± 0.2	9.8 ± 0.2	0.99 ± 0.13
T112	L11/12	−3.78	−3.82	−3.64	−3.50	−3.41	−3.40	−3.27	7.0 ± 0.4	7.7 ± 0.9	0.60 ± 0.40
F113	**β12**	**−7.19**	**−6.59**	**−5.92**	**−5.45**	**−4.64**	**−4.32**	**−4.16**	**12.2 ± 1.8**	**11.2 ± 0.2**	**1.70 ± 0.15**
E114	**β12**	**−7.15**	**−6.47**	**−6.12**	**−5.54**	**−4.76**	**−4.31**	**−4.20**	**11.3 ± 1.7**	**10.6 ± 0.4**	**1.59 ± 0.24**
I116	β12	−6.06	−6.01	−5.03	−5.86	−5.08	−4.51	−4.35	nd	7.9 ± 0.7	nd
I118	L12	−4.44	−4.50	−4.54	−4.38	−4.40	−4.41	−4.33	nd	3.9 ± 0.1	nd

[a] Residues classified as global exchangers (see also Figure 1) which form the slow exchange core are shown in bold type. These residues were chosen on the basis of the slowest average exchange rate, the strongest dependence of exchange on denaturant concentration, and the strongest temperature dependence for exchange rates (R. S. Houliston, L. M. R. Singh, and E. M. Meiering, unpublished data). [b] Elements of structure in the protein are numbered from the N- to C-terminus with β-strands designated by β, turns designated by T, and loops or unstructured regions designated by L. [c] Exchange rates were measured at pH 7.8 and 17.4 °C. Error estimates for k_{obs} from the fitting program are typically ∼5−10%. Duplicate measurements of k_{obs} for 0 M urea gave rates that generally agreed within error estimates of the fitting program. [d] Values for ΔG_{op}^{loc}, ΔG_{op}^{glob}, and m^{glob} were obtained by calculating ΔG_{ex} for k_{obs} values from 0 to 2 M urea using eq 5, and then fitting ΔG_{ex} vs urea concentration to eq 6, with ΔG_{op}^{loc} and ΔG_{op}^{glob} equal to $-RT \ln K_{op}^{loc}$ and $-RT \ln K_{op}^{glob}$, respectively. Error estimates for the fitted parameters are from the fitting program. Parameters that could not be fit using eq 6 are marked nd. For I116 and I118, values of ΔG_{ex} changed very little with urea concentration, and could not be fit using eq 6; values for ΔG_{op}^{glob} for these residues represent the average value of ΔG_{ex} for 0−2 M urea.

abrupt change in slope for these amides at ∼2 M urea suggests that below 2 M urea exchange is dominated by EX2. Similar abrupt changes from EX2 to EX1 exchange have also been seen for other proteins (*38*, *40*). Since the more rapidly exchanging amides tend more toward EX2 than the slower exchanging amides in hisactophilin (Figure 6) and other proteins (see refs *32* and *41* and the Discussion), we have analyzed the data for 0−2.0 M urea for all amides in hisactophilin using EX2-based structural unfolding models.

Analysis of Exchange Rates Using Structural Unfolding Models. Exchange data for 0−2.0 M urea are well fit by eq 6 for a two-process structural unfolding model (Figure 8). Values of ΔG_{op}^{glob}, m^{glob}, and ΔG_{op}^{loc} from the fits are summarized in Table 3. There is a large spread in fitted values for different amides, with ΔG_{op}^{glob}, ΔG_{op}^{loc}, and m^{glob} tending to be largest for amides with the smallest k_{obs} values. Values of ΔG_{op}^{glob} and m^{glob} for the slowest exchanging amides (Table 3) are similar to ΔG_u^o and m^{glob} values measured by urea denaturation (Table 1), as expected for exchange via global unfolding. The m^{glob} values are somewhat lower for the amide exchange experiments, probably due to some occurrence of EX1.

Apart from the slowest exchangers, amides with similar values of ΔG_{op}^{glob} and m^{glob} are not spatially close together within elements of secondary or tertiary structure; i.e., there is no clear convergence to common subglobal unfolding isotherms for groups of amides localized in different parts of the hisactophilin structure, and hence, partially folded intermediates in which sections of structure are cooperatively disrupted are not clearly apparent. It is possible that some occurrence of EX1 may limit the observation of equilibrium intermediates for hisactophilin, as was the case for the protein barnase (*39*, *40*). The occurrence of EX1 should not, however, fully obscure convergence to subglobal isotherms in hisactophilin because (1) the switch from EX2 to EX1 appears to be quite abrupt (Figure 7) [also for other proteins (*38*, *40*)], and so effects of EX1 should be limited below the switch point; (2) EX1 exchange is most pronounced for

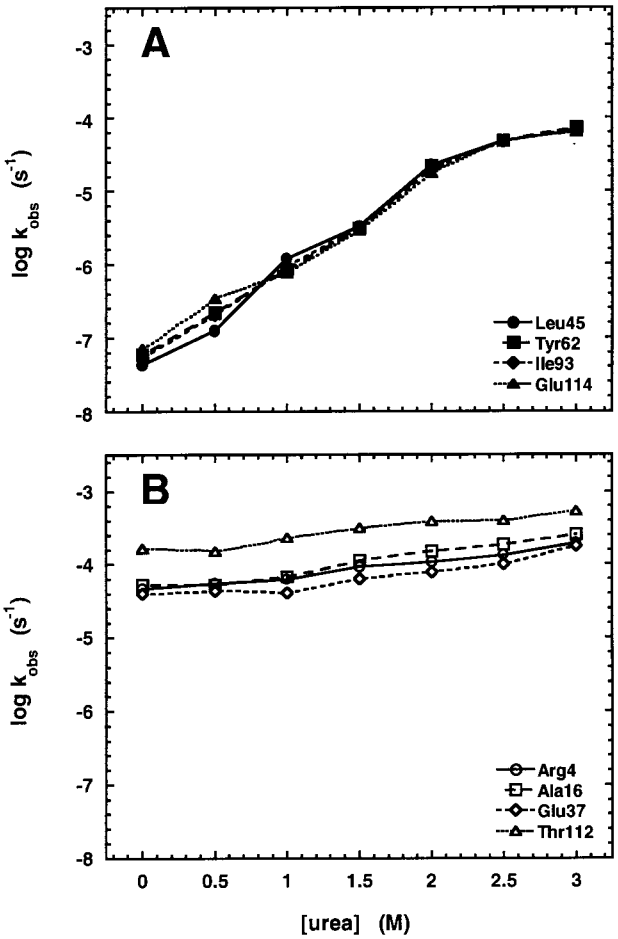

FIGURE 7: Representative urea dependence of amide exchange rates in hisactophilin. (A) Slowly exchanging amides (black symbols) exhibit a strong, essentially linear dependence of exchange rates from 0 to ~2 M urea, and a weaker urea dependence above 2 M urea. (B) Rapidly exchanging amides (white symbols) exhibit a weak, linear dependence of exchange rates over the entire range of urea concentrations. For clarity, lines are drawn connecting data points for each residue.

the slowest exchangers, while more rapidly exchanging amides are more likely to undergo EX2 exchange (Figure 6); and (3) the spread in k_{int} for all the amides analyzed is small (~15-fold), and hence differences in k_{int} should not mask common trends in exchange behavior.

It has been proposed recently that exchange data in urea can be interpreted in terms of exchange from a continuum of states with varying amounts of structure, rather than from discrete partially folded intermediates (*42*, *43*). This proposal is based on the observation that in some proteins there is a continuous distribution of ΔG_{op}^{glob} values which are strongly correlated with m^{glob} values. For hisactophilin, there is also a strong correlation between ΔG_{op}^{glob} and m^{glob} (Figure 9). The existence of this correlation is an additional indication that EX1 does not have a large effect on fitted values of ΔG_{op}^{glob} and m^{glob}.

DISCUSSION

Correlation of Exchange Rates with Protein Structure. To gain insight into the nature of structural fluctuations occurring for different amides, trends in k_{obs} values with respect to the structure of hisactophilin were investigated. Average values of k_{obs} are plotted versus the distance from the amide proton

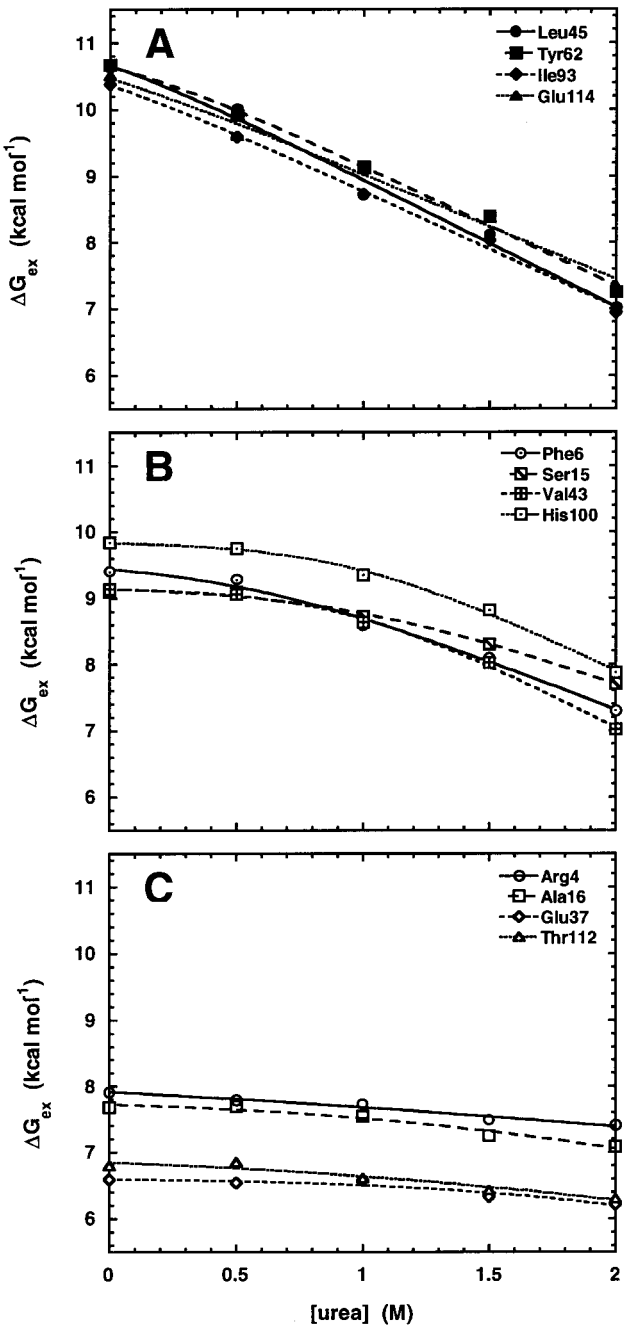

FIGURE 8: Representative urea dependence of the apparent Gibbs free energy of opening for amides in hisactophilin for (A) slowly exchanging amides, (B) intermediate exchanging amides, and (C) rapidly exchanging amides. Lines represent the fits of the data to a two-process structural opening model (eq 6). Values of ΔG_{op}^{loc}, ΔG_{op}^{glob}, and m^{glob} for the fits are summarized in Table 3.

in the folded protein to the closest solvent point in Figure 10. For hisactophilin, there is a weak correlation of k_{obs} with distance to solvent, as has been observed for other proteins (*9*, *14*, *32*). All of the relatively rapidly exchanging amides in hisactophilin are close to the protein surface; however, slowly exchanging amides have a much wider range of distances to solvent. Many of the slowest exchanging amides are situated in the second trefoil unit (e.g., A44, L45, K46, S54, Y62, and F74 in strands 5−8); however, some slow exchangers are also found in the first trefoil (e.g., L14 in strand 2) and in the third trefoil (e.g., I85, K86, I93, S94, F113, and G114 in strands 9, 10, and 12). The slow

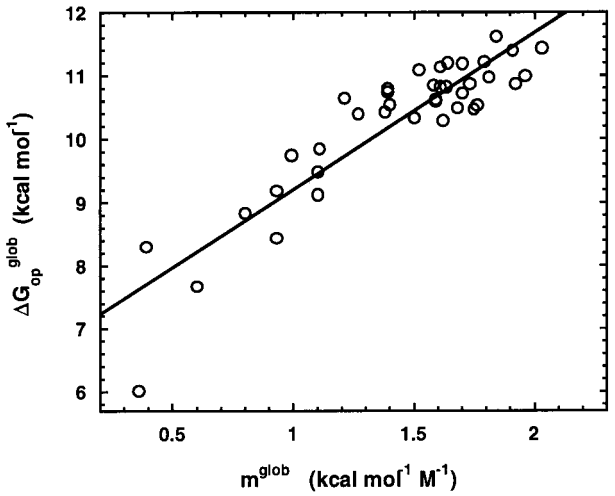

FIGURE 9: Correlation of ΔG_{op}^{glob} and m^{glob} values in hisactophilin. Values of ΔG_{op}^{glob} and m^{glob} (Table 3) obtained from fitting exchange data to a two-process structural opening model (eq 6) exhibit a strong correlation ($R = 0.90$) when the data are fit to a straight line by nonlinear least-squares regression.

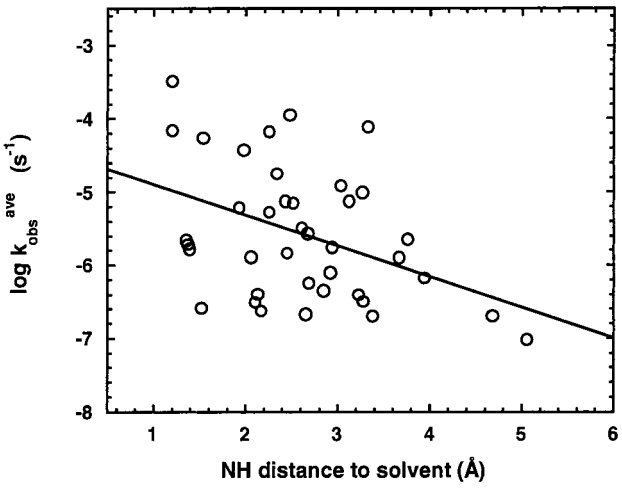

FIGURE 10: Average exchange rate vs the distance from the amide proton to solvent in the solution structure of hisactophilin. Log k_{obs} is the average value for data from pH 6.8 to 8.7. Distances were determined using the solution structure of hisactophilin [PDB entry 1hcd (*3*)], and a Connolly surface generated using the program InsightII (MSI). There is a weak correlation between the average exchange rate and the distance to the solvent when the data are fit to a straight line by nonlinear least-squares regression ($R = 0.42$).

exchangers are concentrated near the interface of the β-barrel and β-hairpin triplet portions of the structure (Figure 1), which we therefore consider to be the "slow exchange core" of hisactophilin.

Comparisons of amide exchange behavior for proteins from different superfamilies with the same fold may reveal trends in local and global stability and provide insight into how diverse primary sequences can adopt the same overall structure. Amide exchange rates have been reported for one other β-trefoil protein, IL-1β (*44*). As for hisactophilin, the slowest exchanging amides in IL-1β are distributed throughout the primary sequence, and are concentrated in the second trefoil and at the β-barrel−β-hairpin triplet interface. Thus, the overall exchange behavior and slow exchange core seem to be conserved between these two β-trefoil proteins. Comparisons of exchange behavior among other proteins in different fold families have yielded varying results. For proteins that adopt the OB fold, amides in nonconserved structural elements tend to exhibit faster exchange rates whereas amides in the conserved, central β-portion of the structure exchange most slowly and form a conserved "slow exchange core" (*45*). For different superfamilies that adopt a flavodoxin-like fold, the "stable nucleus" of slowly exchanging amides may be conserved between cutinase (*46*) and CheY (*47*), but it is different in flavodoxin (*48*). It is interesting that the location of very slow exchangers appears to be conserved in the OB and β-trefoil folds, which have a single conserved hydrophobic core formed by β-structure, but it is apparently not maintained in the flavodoxin fold, which contains various α-helices and has more than one hydrophobic core. These results suggest that the positions of the slowest exchangers may tend to be more highly conserved in β-structures containing a single hydrophobic core.

Rate Constants of Opening and Closing. In-depth analyses of k_{op} and k_{cl} values have now been reported for four proteins: lysozyme (*32*), turkey ovomucoid third domain (OMTKY3) (*17*, *41*), acyl coenzyme A binding protein (ACBP) (*49*), and hisactophilin. It is of interest to examine trends in k_{op} and k_{cl} among these proteins. In all four proteins, decreasing k_{obs} is clearly correlated with decreasing k_{op}; i.e., the slowest exchanging amides have the slowest opening rates, and hence, global opening or unfolding tends to be much slower than local unfolding. Rates of global unfolding measured by amide exchange are in good agreement with rates measured by optical or saturation transfer methods (Tables 1 and 2; *19* and references therein). Thus, amide exchange measurements seem to give reliable values of k_{op}, and clear trends in k_{op} can be identified.

Trends in k_{cl}, however, are considerably less clear than trends in k_{op}. In all four proteins, amides with the smallest values of k_{op} tend also to have the smallest values of k_{cl}, indicating that global closing is slower than local closing. This trend is not very strong, though, for lysozyme, and for OMTKY3, the trend is reversed when considering only relatively rapidly exchanging amides (*41*). Rates for the relatively rapidly exchanging amides are considerably faster than rates for the other amides under consideration here, and rates for the rapid exchangers were determined using quenched-flow exchange experiments; all other rates were determined by measuring spectra as a function of time after dissolution of protein in D_2O. The two types of experiments may therefore tend to be sensitive to different processes in proteins. Values of k_{cl} tend to be smallest for the slowest exchanging amides in hisactophilin (Table 2 and Figure 6) and OMTKY3 (*17*, *41*), but for ACBP, lysozyme, and the faster exchanging group of amides in OMTKY3, there is a weak tendency for k_{cl} to be larger for the slowest exchanging amides. There is no apparent correlation between values of k_{cl} or k_{op} and global protein stability. For example, although OMTKY3 is more stable (*17*) than ACBP (*49*), it also has much higher values for both k_{op} and k_{cl}. In general, correlations of k_{op} and k_{cl} with stability are not expected because rates are not necessarily correlated with equilibrium populations (*10*, *20*).

As pointed out above (see the Results), there may be difficulties in determining accurate values of k_{cl} and, hence, in identifying trends in k_{cl}, due to possible inaccuracies in k_{int}. Values of k_{cl} for global folding measured by amide

exchange and other methods (Tables 1 and 2; *19* and references therein) agree within ~10-fold, suggesting that k_{int} in the globally open state can be predicted quite accurately using values of k_{int} determined for model peptides (*21*). However, non-hydrogen-bonded surface amides in the native protein may exchange up to 3 orders of magnitude more slowly than predicted on the basis of model peptides (*11*, *50*); hence, errors in k_{int} for locally exchanging amides may be larger than for globally exchanging amides. For hisactophilin, values of k_{op} are significantly correlated with m^{glob}, ΔG_{op}^{glob}, and ΔG_{op}^{loc} ($R = 0.76$, 0.75, and 0.87, respectively) while values of k_{cl} are much less correlated with these parameters ($R = 0.47$, 0.32, and 0.27, respectively). The lower correlation coefficients for k_{cl} may be related to some as yet unidentified property of hisactophilin, or they may be caused by inaccuracies in k_{int}. Further studies are required to rationalize the values obtained for k_{cl} in different proteins.

Exchange Mechanism. Experiments on many different proteins have revealed that generally EX2 is the dominant exchange mechanism for backbone amides in proteins, except under extreme or destabilizing conditions such as high pH or high temperature (*14*, *51*). Recently, however, there have been a number of studies reporting EX1 exchange for the slowest exchanging amides in proteins under relatively mild solution conditions, i.e., at moderate temperatures and pHs where proteins are quite stable (reviewed in ref *10*). In some cases, a contribution of EX1 to exchange for these amides can result in "overprotection"; i.e., $\Delta G_{ex} > \Delta G_u^o$ (*52*, *53*). Overprotection can also be caused by other factors, however, such as proline isomerization, exchange from a high-energy open state, and overestimation of k_{int} (*10*).

For hisactophilin, overprotection for the slowest exchangers is apparent at pH 9.7 and 5.9, but not at pH 6.8−8.7. Hisactophilin contains no prolines; hence, these do not affect the exchange analysis. Some of the other factors listed above could in principle be significant; however, the exchange data for hisactophilin in the absence of denaturant can be explained largely in terms of predominantly EX2 exchange at pH 6.8−8.7, with significant contributions of EX1 at pH 9.7 and 5.9. For pH 6.8−8.7, $\Delta G_u^o \approx \Delta G_{ex}$ for the slowest exchangers (Tables 1 and 2 and Supporting Information) and k_{ref} and $k_{cl} > k_{int}$ (Figure 6B), consistent with exchange mainly via EX2. At pH 9.7, the much larger values of k_{int} result in a significant level of EX1 for all amides (Figure 6B). Similarly, EX1 behavior was found to be significant at pH 10 for all amides in OMTKY3 (*41*). In general, EX2 is favored at lower pHs where k_{int} values are lower; however, below pH 6.8, hisactophilin stability decreases markedly and refolding becomes very slow (Table 1). Consequently, EX1 also appears to become significant at pH 5.9. The apparently higher degree of overprotection at pH 5.9 compared to that at pH 9.7 may be caused in part by small differences in solution pH for denaturation curves and amide exchange measurements, since stability is extremely sensitive to solution pH near 5.9 (Table 1; *8*). The occurrence of EX1 exchange for hisactophilin in the absence of denaturant at both high and low pHs emphasizes that EX2 behavior should not be assumed a priori for all amides in a given protein, even under solution conditions where the native state is quite stable.

Identification of Intermediates by Amide Exchange. Native state amide exchange measurements have now been conducted for various proteins with different folds and folding pathways (for reviews, see refs *10*, *11*, and *20*). These measurements identified equilibrium intermediates in which some elements of secondary structure were cooperatively disrupted for some proteins [e.g., cytochrome *c* (*54*), ribonuclease H (*55*), barstar (*56*), apocytochrome b_{562} (*57*), and T4 lysozyme (*42*)] but not for others [e.g., peptostreptococcal protein L (*37*), chymotrypsin inhibitor 2 (*58*), and the relatively large, predominantly β-protein, β-lactoglobulin (*59*)]. Hisactophilin is another example of a protein for which partially unfolded equilibrium intermediates are not apparent in native state exchange experiments. Although there may be some limitations in the detection of intermediates for hisactophilin due to the occurrence of EX1, the lack of clear convergence of amide exchange data to common isotherms suggests that this protein does not form equilibrium intermediates as readily as some other proteins.

When the results obtained for different proteins to date are considered, it appears that partially unfolded intermediates may be detected most readily for proteins that are relatively large and stable, with significant α-helical structure involved in the formation of more than one hydrophobic core. Unfolding of any particular helix may disrupt one core but leave other cores intact, giving rise to relatively stable partially folded intermediates. Hisactophilin, on the other hand, contains a single, large hydrophobic core formed by many long-range interactions between bulky, hydrophobic residues in 12 different β-strands (Figure 1). Since all of the β-strands in hisactophilin are involved in forming the core, there may be little scope for the cooperative disruption of subglobal units of structure, and hence, exchange competent states may be limited to local noncooperative perturbations in structure and cooperative global unfolding.

For some proteins, equilibrium intermediates have a strong resemblance to kinetic folding intermediates, while for other proteins, this is not observed (reviewed in refs *10*−*12* and *20*). Optical and quenched-flow NMR experiments indicate that under stabilizing solution conditions hisactophilin forms a kinetic folding intermediate (Figure 2), in which strands 4−8 fold first while strands 1−3 and 10−12 form last (*22*). Intermediates are not very prominent in equilibrium or kinetic experiments on hisactophilin, making in-depth structural comparisons difficult. On the whole, though, there is a weak tendency for amides that exchange most slowly in the native state to be protected earliest during folding. Quenched-flow NMR and mass spectrometry experiments (*60*, *61*) and folding simulations (*62*) on IL-1β have shown that folding of this protein also involves formation of an intermediate, which has a topology similar to that of the hisactophilin intermediate, but which is much more prominent during folding. The amides protected in the IL-1β intermediate include many of the amides that exchange most slowly in the native state (*11*, *44*, *60*). Given the prominence of the kinetic intermediate for IL-1β, it would be interesting to see if equilibrium intermediates would also be more apparent for this protein than for hisactophilin. Kinetic intermediates have also been detected for basic and acidic human fibroblast growth factors in optical studies (*63*, *64*). For the acidic growth factor, quenched-flow NMR experiments identified a quite different intermediate in which strands 1 and 12 are

folded first (*63*). Further experiments are in progress in our lab to analyze the stability and nature of the kinetic folding intermediate for hisactophilin and the nature of structural fluctuations at equilibrium under different solution conditions. These experiments will provide further insights into formation of intermediates by β-trefoil proteins, and the role of specific interactions in differential stabilization of intermediates.

ACKNOWLEDGMENT

We thank Drs. Mike Sauder, Yu-Zhu Zhang, and Heinrich Roder for providing the HX-predict program and Greg Clarke for assistance with the computer analysis of the data.

SUPPORTING INFORMATION AVAILABLE

Plot of ΔG_{ex} versus pH for slowly exchanging backbone amides in hisactophilin (Table 1). This material is available free of charge via the Internet at http://pubs.acs.org.

REFERENCES

1. Scheel, J., Ziegelbauer, K., Kupke, T., Humbel, B. M., Noegel, A. A., Gerisch, G., and Schleicher, M. (1989) *J. Biol. Chem. 264*, 2832−2839.
2. Schleicher, M., Andre, B., Andreoli, C., Eichinger, L., Haugwitz, M., Hofmann, A., Karakesisoglou, J., Stockelhuber, M., and Noegel, A. A. (1995) *FEBS Lett. 369*, 38−42.
3. Habazettl, J., Gondol, D., Wiltscheck, R., Otlewski, J., Schleicher, M., and Holak, T. A. (1992) *Nature 359*, 855−858.
4. Murzin, A. G., Lesk, A. M., and Chothia, C. (1992) *J. Mol. Biol. 223*, 531−543.
5. Murzin, A. G., Brenner, S. E., Hubbard, T., and Chothia, C. (1995) *J. Mol. Biol. 247*, 536−540.
6. Ponting, C. P., and Russell, R. B. (2000) *J. Mol. Biol. 302*, 1041−1047.
7. Hammond, M. S., Houliston, R. S., and Meiering, E. M. (1998) *Biochem. Cell Biol. 76*, 294−301.
8. Liu, C., Chu, D., Wideman, R., Houliston, R. S., Wong, H. J., and Meiering, E. M. (2001) *Biochemistry 40*, 3817−3827.
9. Englander, S. W., and Kallenbach, N. R. (1983) *Q. Rev. Biophys. 16*, 521−655.
10. Clarke, J., and Itzhaki, L. S. (1998) *Curr. Opin. Struct. Biol. 8*, 112−118.
11. Li, R., and Woodward, C. (1999) *Protein Sci. 8*, 1571−1590.
12. Englander, S. W. (2000) *Annu. Rev. Biophys. Biomol. Struct. 29*, 213−238.
13. Linderstrom-Lang, K. U. (1955) *Spec. Publ.—Chem. Soc. 2*, 1−20.
14. Hvidt, A., and Nielsen, S. O. (1966) *Adv. Protein Chem. 21*, 287−386.
15. Tanford, C. (1970) *Adv. Protein Chem. 24*, 1−95.
16. Roder, H., Wagner, G., and Wuthrich, K. (1985) *Biochemistry 24*, 7396−7407.
17. Arrington, C. B., and Robertson, A. D. (1997) *Biochemistry 36*, 8686−8691.
18. Arrington, C. B., and Robertson, A. D. (2000) *Methods Enzymol. 323*, 104−124.
19. Sivaraman, T., Arrington, C. B., and Robertson, A. D. (2001) *Nat. Struct. Biol. 8*, 331−333.
20. Chamberlain, A. K., and Marqusee, S. (2000) *Adv. Protein Chem. 53*, 283−328.
21. Bai, Y., Milne, J. S., Mayne, L., and Englander, S. W. (1993) *Proteins 17*, 75−86.
22. Liu, C., Gaspar, J. A., Wong, H. J., and Meiering, E. M. (2002) *Protein Sci.* (in press).
23. Oliveberg, M., Tan, Y. J., Silow, M., and Fersht, A. R. (1998) *J. Mol. Biol. 277*, 933−943.
24. Viguera, A. R., Martinez, J. C., Filimonov, V. V., Mateo, P. L., and Serrano, L. (1994) *Biochemistry 33*, 2142−2150.
25. Matouschek, A., Matthews, J. M., Johnson, C. M., and Fersht, A. R. (1994) *Protein Eng. 7*, 1089−1095.
26. Meiering, E. M., Li, H., Delcamp, T. J., Freisheim, J. H., and Wagner, G. (1995) *J. Mol. Biol. 247*, 309−325.
27. Zhang, Y.-Z. (1995) Ph.D. Thesis, University of Pennsylvania, Philadelphia, PA.
28. Antonino, L. C., Kautz, R. A., Nakano, T., Fox, R. O., and Fink, A. L. (1991) *Proc. Natl. Acad. Sci. U.S.A. 88*, 7715−7718.
29. Kuhlman, B., and Raleigh, D. P. (1998) *Protein Sci. 7*, 2405−2412.
30. Makhatadze, G. I., Clore, G. M., and Gronenborn, A. M. (1995) *Nat. Struct. Biol. 2*, 852−855.
31. Parker, M. J., and Clarke, A. R. (1997) *Biochemistry 36*, 5786−5794.
32. Pedersen, T. G., Thomsen, N. K., Andersen, K. V., Madsen, J. C., and Poulsen, F. M. (1993) *J. Mol. Biol. 230*, 651−660.
33. Roder, H., Wagner, G., and Wuthrich, K. (1985) *Biochemistry 24*, 7407−7411.
34. Robertson, A. D., and Baldwin, R. L. (1991) *Biochemistry 30*, 9907−9914.
35. Arcus, V. L., Vuilleumier, S., Freund, S. M., Bycroft, M., and Fersht, A. R. (1994) *Proc. Natl. Acad. Sci. U.S.A. 91*, 9412−9416.
36. Radford, S. E., Buck, M., Topping, K. D., Dobson, C. M., and Evans, P. A. (1992) *Proteins 14*, 237−248.
37. Yi, Q., Scalley, M. L., Simons, K. T., Gladwin, S. T., and Baker, D. (1997) *Folding Des. 2*, 271−280.
38. Loh, S. N., Rohl, C. A., Kiefhaber, T., and Baldwin, R. L. (1996) *Proc. Natl. Acad. Sci. U.S.A. 93*, 1982−1987.
39. Clarke, J., and Fersht, A. R. (1996) *Folding Des. 1*, 243−254.
40. Dalby, P. A., Clarke, J., Johnson, C. M., and Fersht, A. R. (1998) *J. Mol. Biol. 276*, 647−656.
41. Arrington, C. B., and Robertson, A. D. (2000) *J. Mol. Biol. 296*, 1307−1317.
42. Llinas, M., Gillespie, B., Dahlquist, F. W., and Marqusee, S. (1999) *Nat. Struct. Biol. 6*, 1072−1078.
43. Parker, M. J., and Marqusee, S. (2000) *J. Mol. Biol. 300*, 1361−1375.
44. Driscoll, P. C., Gronenborn, A. M., Wingfield, P. T., and Clore, G. M. (1990) *Biochemistry 29*, 4668−4682.
45. Alexandrescu, A. T., Jaravine, V. A., Dames, S. A., and Lamour, F. P. (1999) *J. Mol. Biol. 289*, 1041−1054.
46. Prompers, J. J., Groenewegen, A., Van Schaik, R. C., Pepermans, H. A., and Hilbers, C. W. (1997) *Protein Sci. 6*, 2375−2384.
47. Lacroix, E., Bruix, M., Lopez-Hernandez, E., Serrano, L., and Rico, M. (1997) *J. Mol. Biol. 271*, 472−487.
48. Steensma, E., and van Mierlo, C. P. (1998) *J. Mol. Biol. 282*, 653−666.
49. Kragelund, B. B., Heinemann, B., Knudsen, J., and Poulsen, F. M. (1998) *Protein Sci. 7*, 2237−2248.
50. Tuchsen, E., and Woodward, C. (1985) *J. Mol. Biol. 185*, 405−419.
51. Englander, S. W., Sosnick, T. R., Englander, J. J., and Mayne, L. (1996) *Curr. Opin. Struct. Biol. 6*, 18−23.
52. Swint-Kruse, L., and Robertson, A. D. (1996) *Biochemistry 35*, 171−180.
53. Bai, Y., Milne, J. S., Mayne, L., and Englander, S. W. (1994) *Proteins 20*, 4−14.
54. Bai, Y., Sosnick, T. R., Mayne, L., and Englander, S. W. (1995) *Science 269*, 192−197.
55. Chamberlain, A. K., Handel, T. M., and Marqusee, S. (1996) *Nat. Struct. Biol. 3*, 782−787.
56. Bhuyan, A. K., and Udgaonkar, J. B. (1998) *Proteins 30*, 295−308.

57. Fuentes, E. J., and Wand, A. J. (1998) *Biochemistry 37*, 3687−3698.
58. Itzhaki, L. S., Neira, J. L., and Fersht, A. R. (1997) *J. Mol. Biol. 270*, 89−98.
59. Ragona, L., Fogolari, F., Romagnoli, S., Zetta, L., Maubois, J. L., and Molinari, H. (1999) *J. Mol. Biol. 293*, 953−969.
60. Varley, P., Gronenborn, A. M., Christensen, H., Wingfield, P. T., Pain, R. H., and Clore, G. M. (1993) *Science 260*, 1110−1113.
61. Heidary, D. K., Gross, L. A., Roy, M., and Jennings, P. A. (1997) *Nat. Struct. Biol. 4*, 725−731.
62. Clementi, C., Jennings, P. A., and Onuchic, J. N. (2000) *Proc. Natl. Acad. Sci. U.S.A. 97*, 5871−5876.
63. Samuel, D., Kumar, T. K., Balamurugan, K., Lin, W. Y., Chin, D. H., and Yu, C. (2001) *J. Biol. Chem. 276*, 4134−4141.
64. Estape, D., and Rinas, U. (1999) *J. Biol. Chem. 274*, 34083−34088.
65. Koradi, R., Billeter, M., and Wuthrich, K. (1996) *J. Mol. Graphics 14*, 51−55.

BI0115838